Economic Optimization of a Concentrating Solar Power Plant With Molten-Salt Thermocline Storage

Scott M. Flueckiger
School of Mechanical Engineering,
Purdue University,
585 Purdue Mall,
West Lafayette, IN 47907-2088

Brian D. Iverson
Department of Mechanical Engineering,
435 Crabtree Building,
Brigham Young University,
Provo, UT 84602

Suresh V. Garimella[1]
School of Mechanical Engineering,
Purdue University,
585 Purdue Mall,
West Lafayette, IN 47907-2088
e-mail: sureshg@purdue.edu

System-level simulation of a molten-salt thermocline tank is undertaken in response to year-long historical weather data and corresponding plant control. Such a simulation is enabled by combining a finite-volume model of the tank that includes a sufficiently faithful representation at low computation cost with a system-level power tower plant model. Annual plant performance of a 100 MW_e molten-salt power tower plant is optimized as a function of the thermocline tank size and the plant solar multiple (SM). The effectiveness of the thermocline tank in storing and supplying hot molten salt to the power plant is found to exceed 99% over a year of operation, independent of tank size. The electrical output of the plant is characterized by its capacity factor (CF) over the year, which increases with solar multiple and thermocline tank size albeit with diminishing returns. The economic performance of the plant is characterized with a levelized cost of electricity (LCOE) metric. A previous study conducted by the authors applied a simplified cost metric for plant performance. The current study applies a more comprehensive financial approach and observes a minimum cost of 12.2 ¢/kWh_e with a solar multiple of 3 and a thermocline tank storage capacity of 16 h. While the thermocline tank concept is viable and economically feasible, additional plant improvements beyond those pertaining to storage are necessary to achieve grid parity with fossil fuels. [DOI: 10.1115/1.4025516]

Keywords: thermocline energy storage, concentrating solar thermal power, molten salt, power tower, economic analysis

1 Introduction

Molten-salt thermocline tanks offer a low-cost thermal energy storage option for Concentrating Solar Power (CSP) systems. Unlike conventional two-tank storage, a thermocline tank stores excess hot and cold heat transfer fluid (HTF) inside a single tank volume to avoid the physical redundancy of a second storage tank. Vertical stratification of the hot and cold regions is sustained via fluid buoyancy forces. The resultant fluid interface is an intermediate layer of high-temperature gradient known as the thermocline or heat-exchange region. In addition to the HTF, a thermocline tank also is filled with granulated solid to minimize excess HTF volume required for storage and to mitigate fluid mixing forces detrimental to thermal stratification. Conventional HTFs in solar thermal systems include synthetic oils and molten salts. At present, molten salts are preferable due to lower cost and higher liquid operating temperatures up to 600 °C.

Dispatch of both hot and cold molten salt from the thermocline to the surrounding infrastructure requires fluid ports at the top and bottom of the tank, illustrated in Fig. 1. During daylight, the solar receiver supplies hot molten salt to the top of the tank. At the same time, cold salt exits the bottom of the tank and is returned to the receiver. The tank reaches a fully energized or charged state when the intermediate heat-exchange region reaches the tank floor. During nighttime or cloud transients, the stored energy inside the tank is retrieved via flow reversal. The hot salt is now extracted from the top and delivered to the power block for steam generation, while cold salt returned from the power block enters the tank at the bottom. The process continues until the volume of hot salt inside the tank is exhausted, indicated by a drop in molten-salt temperature exiting the tank.

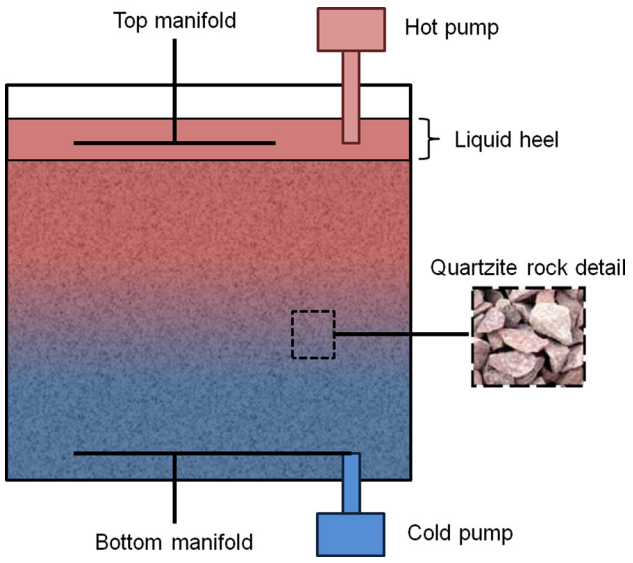

Fig. 1 Schematic illustration of a molten-salt thermocline tank, including the porous quartzite rock bed and the liquid heel. Hot salt is supplied at the liquid heel through the top manifold and is extracted via the hot pump. Cold salt enters the porous bed through the bottom manifold but is also extracted through the manifold via the cold pump.

[1]Corresponding author.

Contributed by the Solar Energy Division of ASME for publication in the Journal of Solar Energy Engineering. Manuscript received May 28, 2013; final manuscript received August 14, 2013; published online October 25, 2013. Assoc. Editor: Nathan Siegel.

Examples of thermocline storage technology include a 170 MWh_t tank that was installed at the historic Solar One pilot plant in Daggett, CA [1]. The tank, containing Caloria HT-43 mineral oil and granite rock, supplied the power plant with heat for auxiliary steam generation during the mideighties. Sandia National Laboratories later constructed a small 2.3 MWh_t thermocline tank, composed of molten salt with quartzite rock and silica sand filler [2]. The concept was again validated as a viable storage option for CSP systems and estimated to provide a 33% cost savings relative to baseline two-tank storage.

Elevated temperatures and the large physical scale of the thermocline tank concept have constrained a majority of recent investigations to computational analysis. Yang and Garimella [3] developed a multidimensional computational fluid dynamics (CFD) model to simulate mass, momentum, and energy transport inside the thermocline tank. Flueckiger et al. [4] later extended this model to simulate hoop stress in the original Solar One thermocline tank and verify the prevention of thermal ratcheting phenomena. Van Lew et al. [5] developed a solution based on the method of characteristics for energy transport inside the thermocline tank. Kolb [6] adopted a system-level modeling approach with a TRNSYS simulation of the 50 MW_e Andasol parabolic trough plant, modified to include a thermocline storage system. Comparison of these various models reveals a persistent tradeoff between comprehensive CFD models with high computing cost and simplified energy transport models with low computing cost. The authors have developed a new thermocline tank model using the finite-volume method to resolve this tradeoff [7]. Integration of this storage model with a system-level power tower plant model enables simulation of year-long thermocline tank performance in response to historical weather data and corresponding plant control.

The contribution of a thermocline tank to CSP plant output is directly related to its energy capacity (or overall size). For a fixed power plant output, larger tanks yield an increased plant capacity factor but require greater capital cost for construction. The amount of thermal energy available for storage is also a function of the power plant solar multiple (maximum thermal power of the solar collection system at noon on summer solstice relative to the heat input required to run the power block). Increasing the solar multiple allows more sunlight to be collected but at the expense of the additional heliostats required. This tradeoff between power production and plant expenditure is characterized by the LCOE. The optimum solar multiple and thermocline tank size is therefore indicated by the minimum LCOE associated with year-long plant operation. A preliminary economic analysis recently performed by the authors was limited to a simplified LCOE metric [8]. The current study updates this analysis with a true LCOE metric obtained from simulating plant performance for varying tank size and solar multiple.

2 Numerical Models

2.1 Thermocline Tank. Simulation of the thermocline is performed with a commercial salt mixture (60% by weight $NaNO_3$, 40% by weight KNO_3) known as solar salt. The salt is liquid above 220 °C; however, the enforced operating span is 300 °C–600 °C to avoid any unwanted salt freezing in the plant infrastructure. While current solar receivers are limited in upper temperature to 565 °C, it is assumed that improvements in future receiver design will satisfy the increased temperature span. Physical properties of the salt in the liquid region are known functions of temperature (degrees Celsius) [9]

$$\rho_l = 2090 - 0.636T_l \tag{1}$$

$$k_l = 0.443 + 1.9 \times 10^{-4}T_l \tag{2}$$

$$\mu_l = 0.022714 - 1.20 \times 10^{-4}T_l + 2.281 \times 10^{-7}T_l^2 - 1.474 \times 10^{-10}T_l^3 \tag{3}$$

The molten-salt specific heat is approximated as a constant value of 1520 J/kg K, which exhibits a maximum error of 1.7% compared to experimental data in the operating temperature span. Quartzite rock is selected as the granulated filler material with density, specific heat, and thermal conductivity assumed to be constant at 2500 kg/m^3, 830 J/kg K, and 5 W/m K, respectively [3,10]. The porosity of the quartzite rock bed is fixed at 0.22 based on observation in past experimental tanks [2]. The filler particle size is also fixed to an effective diameter of 1 cm [11].

For simulation, the temperature of the molten salt and quartzite inside the thermocline tank is normalized with respect to the hot and cold operating limits stated above

$$\Theta = \frac{T - T_c}{T_h - T_c} \tag{4}$$

Assuming a well-insulated tank wall, energy transport in the porous region (fluid and solid) is one-dimensional and characterized by the following equations [3,7]:

$$\frac{\partial(\varepsilon\rho_l C_{p,l}\Theta_l)}{\partial t} + \frac{\partial(\rho_l u C_{p,l}\Theta_l)}{\partial x} = \frac{\partial}{\partial x}\left(k_{eff}\frac{\partial\Theta_l}{\partial x}\right) + h_i(\Theta_s - \Theta_l) \tag{5}$$

$$\frac{\partial[(1-\varepsilon)\rho_s C_{p,s}\Theta_s]}{\partial t} = -h_i(\Theta_s - \Theta_l) \tag{6}$$

A finite-volume solution to these equations is discussed in detail in Ref. [7], including model validation with experimental temperature data reported in the literature [2]. Forced convection between the liquid salt and rock is simulated with the Wakao and Kaguei correlation [12]. Effective thermal conductivity in the liquid phase is characterized with the Gonzo correlation [13]. Spatial discretization of the convective flux term in Eq. (5) is resolved with a quadratic flux limiter function, a quasi-second-order local extrema diminishing scheme. Temporal discretization is performed with a first-order implicit method. Picard iteration is implemented to resolve the nonlinearity in Eq. (5) as well as the interstitial convection coupling in Eq. (6). The resultant algebraic equations are then solved at each time step with a tridiagonal matrix algorithm written in C. Solution iterations are performed at each time step until the nondimensional residual error reduces to less than 10^{-6}. Unlike other energy transport models of thermocline tanks presented in the literature, the current approach accounts for both thermal diffusion and variations in molten-salt density with temperature.

Given that the density of molten salt is a function of temperature, the liquid level inside the thermocline tank is not constant in time. Charging the tank with hot salt raises the liquid level, while discharging the tank (by adding higher-density cold salt) lowers the liquid level. Therefore, a liquid region of molten salt must be maintained above the quartzite rock to prevent porous region dry-out, illustrated in Fig. 1. In reality, the thermal gradient or heat-exchange region of the molten-salt will extend into this heel as the storage tank approaches a fully discharged state. However, a finite-volume solution of the liquid heel is prohibited as the heel thickness varies with time. As a conservative approximation, the heel is instead treated as an isothermal mass. The characteristic temperature of the heel is calculated at each time step from the known mass and energy inside the heel as

$$T_{heel} = T_c + \frac{E_{heel}}{m_{heel}C_{p,l}} \tag{7}$$

It should be noted that hot molten salt delivered to the power block is extracted from the heel. Thus, the instantaneous heel temperature also controls the quality of steam generation and corresponding work output from the CSP plant.

2.2 Power Tower Plant. Simulation of the entire CSP plant is achieved by coupling the thermocline tank model described above with a solar collection model and a power block model. Solar collection of direct sunlight is performed with a power tower design. A surround field of dual-axis heliostats follows the position of the sun and reflects the direct normal irradiance (DNI) onto an elevated receiver. In conjunction with the thermocline tank operation, molten salt enters the receiver at 300 °C and exits at 600 °C. The corresponding mass flow rate of molten salt is then a function of the current power incident to the receiver

$$\dot{m}_{\text{rec}} = \frac{P_{\text{rec}}}{C_{\text{p,l}}(T_{\text{h}} - T_{\text{rec,in}})} \tag{8}$$

where P_{rec} is adjusted for radiative and convective losses. The thermal rating of the solar receiver is the product of the solar multiple and the Rankine cycle heat input at nameplate or rated load. Sunlight data for the plant simulation are taken from measurements near Barstow, CA, selected for its excellent annual solar resource of 2700 kWh/m^2. Included in this dataset are DNI measurements at 15-min intervals from Jan. 1 to Dec. 31 of 1977. The solar receiver performance is then determined with SOLERGY, a power tower plant performance model developed by Sandia National Laboratories [14].

Power production is modeled with a traditional steam Rankine cycle composed of a nonreheat turbine and a single open feedwater heater, as illustrated in Fig. 2. At the rated load of 100 MW$_e$ net work output, superheated steam enters the turbine at a temperature and pressure of 538 °C and 125 bar (state 1). After the first turbine stage, a fraction of the steam (y) is diverted to the open feedwater heater for deaeration (state 2). The remaining steam travels through the second turbine stage (state 3), is condensed across the vapor dome at 0.1 bar (state 4), and is then pumped to the feedwater heater (state 5). Saturated liquid exits the feedwater heater (state 6) and is then pumped to the heat exchangers (state 7). Recirculation of saturated liquid ($x = 0$) from the evaporator ensures that feedwater always enters the preheater at 230 °C (state 8).

A 10.3% overdesign of the power block is assumed to accommodate any parasitic electrical demands within the power plant [15], equivalent to a gross turbine output of 111.5 MW$_e$. The first-law efficiency of the model cycle at rated load is 0.4116, indicating a necessary heat input of 270.9 MW$_t$. This heat is delivered to the power block via hot molten salt extracted from the thermocline tank. The salt travels through a series of heat exchangers (preheater, evaporator, and superheater) to generate the necessary turbine steam. The size of each heat exchanger is determined from the overall heat transfer coefficients reported for the power block assembly operated at Solar Two [16].

In addition to the rated turbine output, the inclusion of a molten-salt thermocline tank also allows for derated operation.

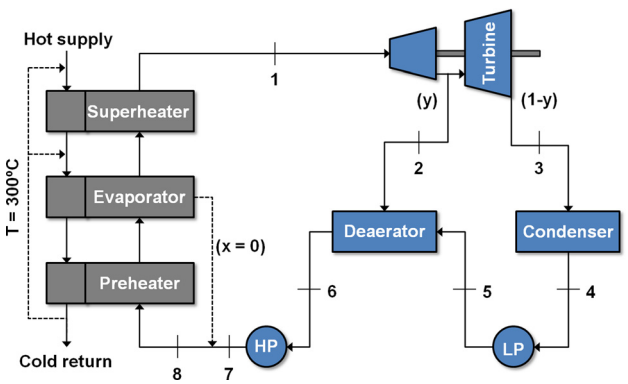

Fig. 2 Steam generators and steam Rankine cycle layout. LP is the low pressure pump and HP is the high pressure pump.

Derated power modes occur in response to molten salt delivered from the thermocline at temperatures below the hot design limit of 600 °C. This reduction in exergy is carried through the subsequent steam generation and reduces the turbine inlet temperature. Power production is sustained so long as the thermodynamic cycle adjusts in response to the decrease in steam quality. In practice, the steam mass flow rates and pressures are both lowered to accommodate the reduced turbine temperature, known as *sliding pressure operation*. Recirculation of cold salt is also enforced in the current study to maintain a saturated mixture inside the evaporator and a fixed amount of superheat at the turbine inlet. Derated operation is also limited to 30% of the rated gross output, associated with a molten-salt supply temperature of 473 °C.

Prior to any power production, both the heat exchangers and the Rankine cycle must be conditioned for operation through a startup process. This process includes warming of the heat exchangers, synchronization of the turbine with the generator, and ramp up to the rated gross output. During the heat exchanger warming and turbine synchronization stage, the thermocline tank supplies hot molten salt to the model power block at the minimum thermal rating, but with no work output. After synchronization is complete, the turbine initiates power production with a linear ramp up to rated operation. The required time interval for these actions is a function of the initial temperature of the turbine, summarized in Table 1. This temperature is given by the amount of time elapsed since the previous shutdown [17].

It should be noted that power tower plants may circulate hot molten salt through the heat exchangers during periods of shutdown to slow the cooling process. The present model omits this mode of operation.

Detailed discussion of the solar collection and power block models as well as system-level integration is available in Ref. [7]. Control of the thermocline tank at the system level is determined by the transient operation of both the solar receiver and the power block. During sunlight hours, the solar receiver activates and supplies hot molten salt to the tank for storage. When a sufficient amount of energy is stored, the tank supplies this hot salt to the power block for steam generation and associated power production. The plant is assumed not to include a storage bypass line between the receiver and power block. The flow direction inside the thermocline tank (charge or discharge) is therefore dictated by the relative operational needs of the solar receiver and the power block. However, additional constraints must be enforced to prohibit excessive, cyclic operation of the thermocline tank or the power block, as discussed below.

Under ideal clear-sky conditions, a tank discharge would only occur at the onset of nighttime during shutdown of the solar receiver. In reality, random cloud transients lead to sporadic DNI losses during daylight hours. Startup of the power block is therefore delayed until the thermocline tank contains at least 2 h of utilizable heat for steam generation in order to prevent excessive wear on either the thermocline tank or the Rankine cycle. As a result, rapid on–off toggling of either the storage system or the Rankine cycle is avoided.

2.3 Levelized Cost of Electricity. The economic viability of a power plant is characterized by its LCOE, or the required power price in ¢/kWh$_e$ needed to offset the entire plant expenditure within its operational lifetime [17,18]

Table 1 Power block startup times for different turbine temperature states

Shutdown, h	Turbine temperature	HX warming, min	Ramp up, min
<12	Hot	15	25
12–72	Warm	60	100
>72	Cold	110	160

$$\text{LCOE} = \frac{\text{TCC} \cdot \text{FCR} + \text{FOM}}{\text{A} \cdot \text{CF} \cdot 8760} + \text{VOM} \quad (9)$$

Total capital cost is the combined direct and indirect costs required for plant construction per rated kilowatt of electric output (¢/kW$_e$). An annual fixed charge rate (FCR) is the percentage of capital cost that must be repaid during each year of operation. The current study assumes an FCR of 7.5% and a plant lifetime of 30 yr, based on previous economic analyses of power tower plants in the literature [17]. The cost per unit energy is dependent on the annual electric output from the plant. This output is governed by the plant availability (A), assumed to be 0.9 according to previous plant predictions [19], and the CF, which is the ratio of power production to the theoretical maximum, i.e., continuous operation at rated load.

Direct capital costs include all tangible resources necessary to build the plant, including site improvements, heliostats, tower, solar receiver, energy storage, power block, balance of plant infrastructure, as well as a contingency to accommodate any unforeseen expenditures. Indirect capital costs include plant design, land, and sales taxes. For the current study, the required land area for the solar plant is assumed to be a circle defined by the radial distance from the central tower to the farthest heliostat. In addition to capital, power plants incur expenditures associated with operation and maintenance. These include fixed operation and maintenance costs that are dependent on plant size and variable operation and maintenance costs that are dependent on electricity generation.

A summary of the various capital and operation costs for a molten-salt power tower plant are taken from System Advisor Model, a financial model for CSP plant performance developed by the National Renewable Energy Laboratory [20], and listed in Table 2. However, with a molten-salt thermocline tank implemented in place of the conventional two-tank storage option, the default capital cost of thermal energy storage is reduced from \$27/kWh$_t$ to \$20/kWh$_t$ to reflect the financial benefit realized [17]. It should also be noted that the solar tower and solar receiver costs do not exhibit a direct scaling with power, but are determined by the following functions reported in System Advisor Model:

$$\$_{\text{tow}} = 1.927 \times 10^6 \exp\left[\frac{h_{\text{tow}} + 0.5(h_{\text{hel}} - h_{\text{rec}})}{8.85}\right] \quad (10)$$

$$\$_{\text{rec}} = 1.262 \times 10^8 \left(\frac{\pi d_{\text{rec}} h_{\text{rec}}}{1571}\right)^{0.7} \quad (11)$$

3 Results and Discussion

Annual plant simulation is performed for a 100 MW$_e$ solar power tower plant. The plant size (i.e., number of heliostats in the surrounding field) is dictated by the solar multiple, which is varied between 1 and 4 in the current study. The optimized power plant dimensions for each SM of interest are determined with DELSOL, a power tower design tool developed by Sandia National Laboratories [15], and summarized in Table 3. In all cases, the default heliostat size (height of 9.93 m and a reflection area of 95.45 m^2) is applied by DELSOL. While a solar multiple of 1 implies that no excess sunlight is ever collected during plant operation, inclusion of a storage system is still useful as a buffer to fluctuations in DNI from the subsequent power production.

For each solar plant size, the energy capacity of the thermocline tank is varied between 6 and 20 h of available storage time. A volumetric overdesign equivalent to an additional half hour of storage is included in all tanks sizes to accommodate the presence of transitional temperatures below the hot design limit. The actual energy capacity of each tank size is the product of this adjusted storage time and the power block heat input at the rated load of 270.9 MW$_t$.

While the energy capacity of each thermocline tank size is known, the corresponding tank shape remains subject to multiple design constraints. Given the density of the molten salt and quartzite bed, the liquid level inside the thermocline tank cannot exceed 39 ft (11.9 m) to satisfy the bearing capacity of the underlying soil with a typical foundation [21]. The height of each thermocline tank design is fixed at 11 m to accommodate the liquid heel, with the requisite energy capacity achieved through scaling of the tank diameter, as summarized in Table 4. However, the necessary diameters for tank sizes with storage capacity exceeding 14 hours are larger than a practical tank limit of 160 feet (48.8 m) reported in a previous design study [21]. For these cases, thermocline energy storage is assumed to include two smaller tanks operating in parallel.

Prior to each solar plant simulation, the thermocline tank fillerbed and liquid heel are both initialized to the cold molten-salt temperature limit of 300 °C. The fillerbed geometry is discretized with 500 cells along the axial height and a time step of 3 s; model accuracy was previously verified with temperature data reported in the literature [2,7]. Prior to storage simulation, the thermal performance of the heliostat field and solar receiver is first simulated in SOLERGY applying the meteorological-year sunlight data reported near Barstow, CA. The instantaneous power collected by the molten salt in the receiver then serves as input to the thermocline tank and power block models for each time step of simulation. Each plant design and thermocline tank size is then subjected to a full year of operation from Jan. 1 to Dec. 31. The influence of

Table 2 Cost parameters for a molten-salt power tower plant [20]. Storage cost for a thermocline tank is taken from Ref. [17].

Cost	Type	Value	Units
Site improvements	Direct	20	\$/m^2
Heliostats	Direct	180	\$/m^2
Balance of plant	Direct	350	\$/kW (gross)
Power block	Direct	850	\$/kW (gross)
Energy storage	Direct	20	\$/kWh
Tower	Direct	Eq. 10	\$
Receiver	Direct	Eq. 11	\$
Contingency	Direct	7	% of DCC
Plant design	Indirect	11	% of DCC
Land	Indirect	10000	\$/acre
Sales tax	Indirect	4	% of DCC
Fixed	O+M	65	\$/kW-yr
Variable	O+M	0.003	\$/kWh

Table 3 100 MW$_e$ power tower plant dimensions as a function of solar multiple [15]

SM	h_{tow}, m	h_{rec}, m	d_{rec}, m	Mirror area, km^2	Land area, km^2
1	137.5	15	10	0.488	3.34
2	187.5	18	18	0.994	6.21
3	225	21	21	1.53	8.95
4	250	23	23	2.12	11.0

Table 4 Thermocline energy capacity and corresponding tank size

Energy capacity, h	Tank diameter, m	Number of tanks
6	31.9	1
8	36.5	1
10	40.6	1
12	44.2	1
14	47.7	1
16	35.9	2
18	38.1	2
20	40.1	2

the thermocline tank on annual plant performance is characterized in terms of thermal energy discard, plant capacity factor, storage effectiveness, and LCOE as discussed in the remainder of Sec. 3.

3.1 Thermal Energy Discard. For prolonged charge processes, cold molten salt exiting the bottom of the thermocline tank will begin to increase in temperature as the transitional heat-exchange region travels to the tank floor. When this warmed salt enters the solar receiver, an increased receiver mass flow rate is assumed so that the exit hot temperature may be maintained at 600 °C. To prevent overcharging of the storage system, the salt exiting at the tank floor is limited to a maximum allowable temperature of 400 °C. When this occurs, the thermocline tank is designated to be at energy capacity and transitions to a forced standby condition. With no more available storage capacity, the solar receiver can only collect enough energy to satisfy the Rankine cycle steam generation. In effect, the mass flow rate of molten salt (at the hot temperature limit T_h) supplied to the thermocline tank is reduced to exactly balance the hot flow to the steam generators, producing no overall addition of energy to the tank. Heliostats are defocused away from the receiver and some amount of sunlight available for concentration must be forgone; this is known as thermal energy discard. The forced tank standby persists until the solar receiver power output decays near sunset and the energy-saturated tank can then be discharged to sustain rated power production.

A plot of annual thermal energy discard for each solar multiple and thermocline tank size is provided in Fig. 3. Values are normalized with respect to the total amount of sunlight available for collection. As expected, the magnitude of annual discard increases with solar multiple. No thermal energy discard is observed with a solar multiple of 1 for any thermocline tank size, because the plant never collects more sunlight than is needed to operate the power block. In contrast, the larger-sized plants are able to collect excess sunlight, increasing the use of the thermocline tank and leading to instances of storage saturation. As tank size increases, saturation becomes less frequent and the amount of energy discarded for the year converges to zero.

For solar multiples of 3 and 4, it is observed that the rate of convergence slows with increasing tank size. As such, zero thermal energy discard is not observed within the span of tank sizes simulated in the current study. It should be noted that both of these plant designs are large enough to sustain 24-h power production during weather periods of high insolation. When this occurs, increasing the thermocline tank size carries diminishing returns for reducing thermal energy discard as the power block is already operating at maximum performance. Therefore, a thermocline tank size big enough to achieve zero annual discard is not practical for large solar multiples.

3.2 Plant Capacity Factor. When thermal energy discard is reduced with increasing storage size, more solar thermal power is collected in the receiver and then converted to work output. The annual output performance of a power plant is characterized by its capacity factor. These factors are plotted in Fig. 4 for each simulation. As expected, capacity factor increases with the applied solar multiple due to the increased amount of thermal energy collected by the solar receiver.

It should be noted that the total amount of potential work output is dependent on the amount of sunlight collected by the receiver. Thus, each power plant design exhibits a maximum obtainable capacity factor independent of thermal energy storage

$$\mathrm{CF}_{\max} = \frac{Q_{\mathrm{rec}}\,\eta_{\mathrm{cyc}}\,\eta_{\mathrm{par}}}{W_{\mathrm{net}}\,24 \cdot 365} \tag{12}$$

The capacity factor limits for solar multiples from 1 to 4 are 0.266, 0.531, 0.806, and 1.09, respectively. The last value exceeds unity and indicates that a solar multiple of 4 may collect more sunlight than what is needed for continuous year-long power production. In reality, capacity factor cannot exceed unity and the maximum for SM = 4 is therefore reduced to 1. The capacity factor data in Fig. 4 are normalized with respect to the theoretical maximums for each solar multiple and plotted in Fig. 5.

As expected, the normalized capacity factor increases with thermocline tank size because less thermal energy is discarded and more of it is converted to net work output. When the discarded thermal energy reduces to zero, the model data converge to a maximum as observed for the solar multiples of 1 and 2. As discussed in Sec. 3.1, solar multiples of 3 and 4 discard energy for all simulated tank sizes and thus do not exhibit a converged maximum.

It is observed that the maximum normalized capacity factor for SM = 2 (0.983) exceeds the corresponding maximum for SM = 1 (0.941). This is due to the inability of the SM = 1 plant design to

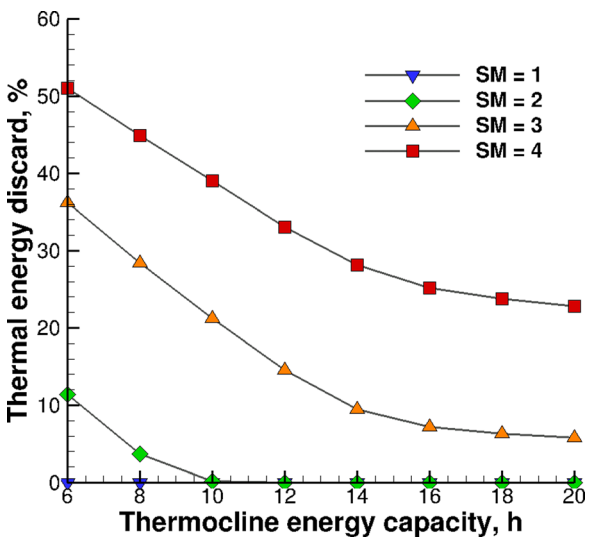

Fig. 3 Annual solar thermal energy discarded due to thermocline tank energy saturation. Values are normalized with respect to the total amount of sunlight available for collection. Plant performance corresponds to weather data recorded near Barstow, CA, for the year 1977.

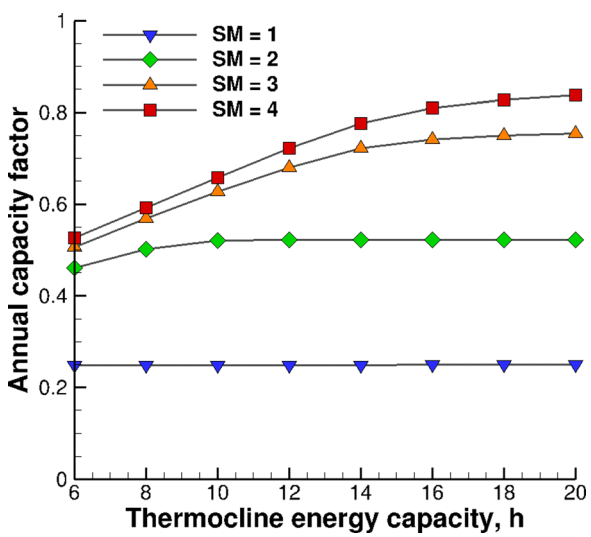

Fig. 4 Annual power tower plant capacity factor. Plant output increases with both solar multiple and thermocline tank energy capacity.

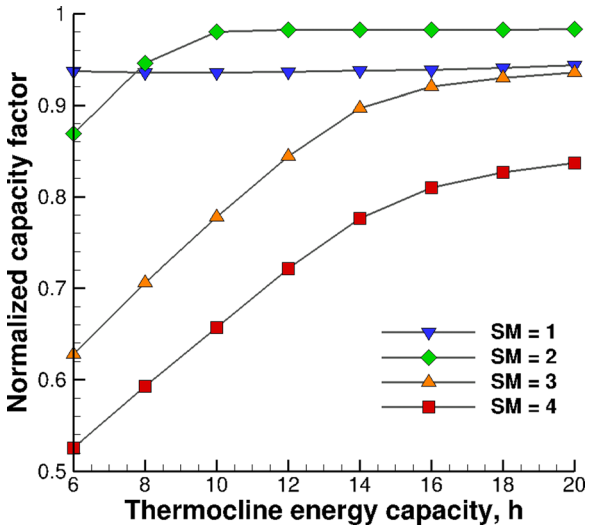

Fig. 5 Annual capacity factor normalized with respect to the theoretical maximum for each solar multiple

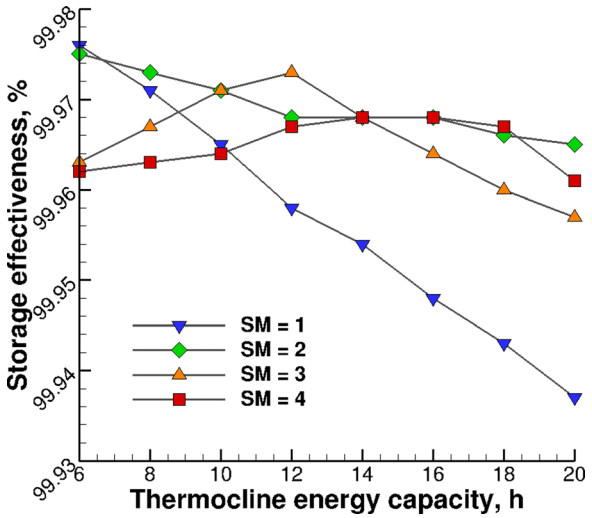

Fig. 6 Annual thermocline tank storage effectiveness. All cases exhibit effectiveness above 99%, validating the thermocline storage concept for implementation in long-term CSP applications.

collect excess sunlight during daylight hours, which then prolongs the daily turbine shutdown periods to an excess of 12 h. As a result, the majority of power block operations require warm turbine startups, which consume more thermal energy than hot startups. Thus, a greater fraction of collected energy is lost to startup in the SM = 1 design than in the SM = 2 design and reduces the normalized capacity factor.

3.3 Storage Effectiveness. As stated previously, the thermocline tank walls are considered well insulated, and are subjected to an adiabatic boundary condition, i.e., no heat is lost from the tank to the surroundings. Without heat loss, the efficiency of the tank remains unity at all times. However, the quality of thermal energy in thermocline storage is not constant as the internal tank temperatures vary with time, including the temperature of the hot salt delivered to the power block. Thus, the storage performance of the tank is instead characterized by an effectiveness metric, as for a heat exchanger. For a thermocline tank, storage effectiveness is defined as the ratio of utilizable heat delivered from the tank to the maximum amount of heat available

$$\varepsilon_{\text{tank}} = \frac{\int \dot{m}_{\text{HX}} C_{\text{p,l}} (T_{\text{heel}} - T_{\text{c}})\, dt}{\int P_{\text{rec}}\, dt} \tag{13}$$

The annual thermocline tank storage effectiveness is plotted in Fig. 6 for each simulation case. All of the simulated tanks exhibit annual storage effectiveness values greater than 99%, indicating that almost all of the thermal energy delivered to the tank from the solar receiver is recovered for steam generation in the power block. Despite adiabatic boundary conditions, the effectiveness exhibits a small loss due to the generation and sustainment of the heat-exchange region between the hot and cold volumes inside the tank. Thus, the molten-salt thermocline tank is a viable thermal energy storage option for long-term operation in a CSP plant, independent of its size.

It should be noted that storage effectiveness is not independent of the time duration assessed in Eq. (13). At shorter durations, the tank is more sensitive to degradation of the thermocline from thermal diffusion and results in lower effectiveness values than that for the yearlong condition applied in Fig. 6. Thermocline effectiveness values for shorter month-long intervals are addressed in Ref. [7].

3.4 Levelized Cost of Electricity. With known plant expenditures and annual capacity factor predictions, the LCOE for each thermocline tank case is calculated with Eq. (9) and plotted in Fig. 7.

The SM = 1 plant design does not exhibit a cost optimum but instead shows a linear increase in cost with thermocline tank size. Without excess solar collection, the thermocline tank for this design size cannot provide a significant benefit to annual power production and only adds to the plant capital cost. It should also be noted that the SM = 1 design yields the largest electricity cost of the four power tower plant designs, verifying that lack of storage utilization is not practical for year-long plant operation. The SM = 2 plant design exhibits a minimum LCOE of 13.4 ¢/kWh$_e$ with a thermocline tank size of 10 h capacity. This size yields almost no thermal energy discard, and thus larger tanks provide little additional benefit and a linear cost increase similar to the SM = 1 plant design is observed. Further, for lower amounts of storage hours (e.g., $\leq$ approximately 10.5 h), plants with an SM = 2 represent the lowest cost option of the four SM values.

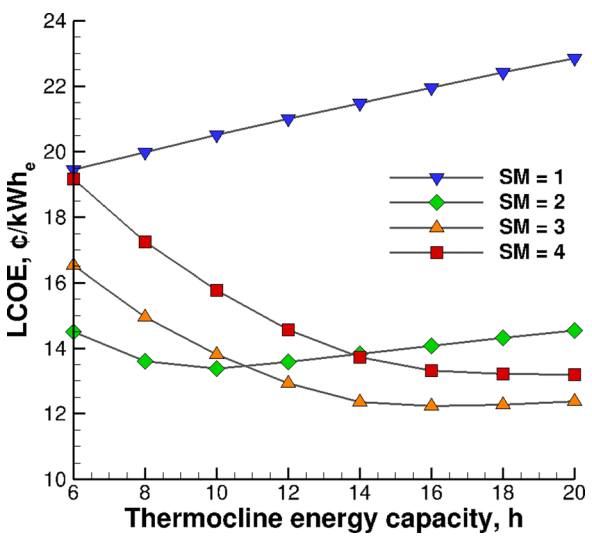

Fig. 7 Levelized cost of electricity for a 100 MW$_e$ power tower plant with thermocline energy storage. Minimum LCOE is observed at a solar multiple of 3 and thermocline energy capacity of 16 hours.

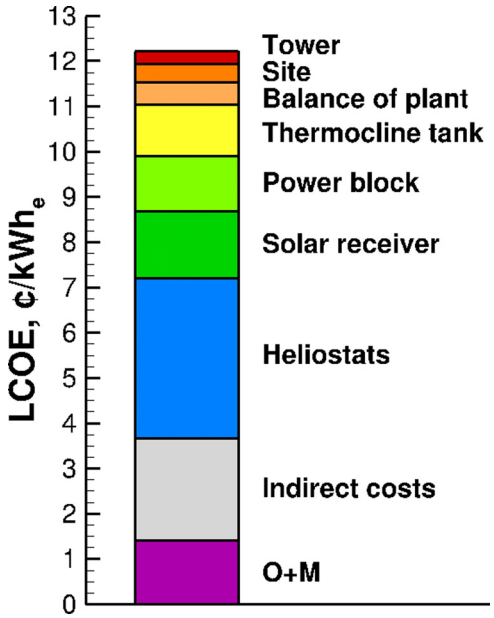

Fig. 8 Individual power tower plant costs at the minimum LCOE of 12.2 ¢/kWh$_e$. Heliostats incur the largest plant capital cost and require improvement to achieve grid parity with fossil fuel.

Greater solar multiples indicate potential for further levelized cost reductions. A solar multiple of 3 exhibits a minimum cost of 12.2 ¢/kWh$_e$ with a thermocline tank size of 16 h capacity. However, a larger multiple of 4 exhibits a minimum cost of 13.2 ¢/kWh$_e$ with a thermocline tank size of 20 h capacity. This increase in cost is explained by the diminishing returns in annual power production observed for increasing solar multiple. At the minimum levelized costs, the capacity factors for the SM = 3 and SM = 4 cases are 0.742 and 0.837, respectively. While the larger solar multiple can provide more annual power, the gain is not sufficient to offset the increase in capital costs required. Thus, a solar multiple of 3 and a thermocline storage capacity of 16 h are found to exhibit an economic optimum for a 100 MW$_e$ molten-salt power tower plant among the cases considered.

The optimum electricity cost of 12.2 ¢/kWh$_e$ identified in this work indicates the extent of cost reduction possible by implementing thermocline energy storage in a power tower plant. However, this minimum does not meet the target price of 6 ¢/kWh$_e$ identified by the U.S. Department of Energy SunShot Initiative [22]. The reason for this discrepancy is illustrated in Fig. 8, which plots the individual contributions of the power tower plant to the levelized cost. The heliostat field is seen to remain a significant capital expenditure and constitutes almost 30% of the total LCOE under the applied economic conditions. The current study is limited to an investigation of thermocline tank size and plant solar multiple. While a thermocline tank offers a useful alternative to two-tank storage, optimization of thermal energy storage alone is not sufficient to achieve domestic grid parity with fossil fuels in the cost of electricity from solar plants. Additional plant improvements outside of thermal energy storage (e.g., heliostat cost reduction) are essential for future power tower plant design.

4 Conclusions

A numerical simulation of a 100 MW$_e$ solar power tower plant is conducted to optimize annual performance as a function of thermocline tank size and plant solar multiple. Thermal energy discard associated with thermocline storage saturation is a strong function of the applied solar multiple. However, for increasing thermocline tank size, less energy is discarded but is instead collected and stored for later power production, as indicated by the annual capacity factor. All tank sizes exhibit high annual storage effectiveness and illustrate the viability of the thermocline tank as a component of future CSP plants.

Economic analysis of the power tower plant indicates a minimum levelized cost of electricity for a solar multiple of 3 and thermocline tank energy capacity of 16 h in the 100 MW$_e$ plant. While larger plants produced more electricity annually, the gain is insufficient to offset the added capital costs. The levelized cost of 12.2 ¢/kWh$_e$ associated with this minimum, updated from a previous simplified economic approach, exceeds the target price of 6 ¢/kWh$_e$, indicating that additional cost reductions outside of thermal energy storage are necessary in a power tower plant to achieve domestic grid parity with fossil fuels.

Acknowledgment

This paper is based upon work supported in part under the US-India Partnership to Advance Clean Energy-Research (PACE-R) for the Solar Energy Research Institute for India and the United States (SERIIUS), funded jointly by the U.S. Department of Energy (Office of Science, Office of Basic Energy Sciences, and Energy Efficiency and Renewable Energy, Solar Energy Technology Program, under Subcontract No. DE-AC36-08GO28308 to the National Renewable Energy Laboratory, Golden, Colorado) and the Government of India, through the Department of Science and Technology under Subcontract IUSSTF/JCERDC-SERIIUS/2012 dated Nov. 22, 2012.

Nomenclature

A = annual plant availability
C_p = specific heat, J/kg K
CF = capacity factor
d = diameter, m
E = energy, J
FCR = fixed charge rate
FOM = fixed operation and maintenance, ¢/kW$_e$
h = height, m
h_i = interstitial convection coefficient, W/m^3 K
k_{eff} = effective thermal conductivity, W/m K
m = mass, kg
P_{rec} = solar receiver incident power, W
Q_{rec} = annual solar receiver absorbed energy, J
SM = solar multiple
t = time, s
T = temperature, °C
TCC = total capital cost, ¢/kW$_e$
u = superficial velocity, m/s
VOM = variable operation and maintenance, ¢/kWh$_e$
W_{net} = net work output, W
x = axial location, m
y = steam fraction for deaeration

Greek Symbols

ε = porosity
ε_{tank} = storage effectiveness
η = efficiency
Θ = normalized temperature
μ = viscosity, Pa s
ρ = density, kg/m^3

Subscripts

c = cold temperature limit
cyc = gross cycle efficiency
e = electric
h = hot temperature limit
heel = thermocline liquid heel
hel = heliostat

HX = power block heat exchangers
l = molten salt region
par = parasitic energy losses
rec = solar receiver
s = solid filler region
t = thermal
tow = tower

References

[1] Faas, S. E., Thorne, L. R., Fuchs, E. A., and Gilbertsen, N. D., 1986, "10 MWe Solar Thermal Central Receiver Plant: Thermal Storage Subsystem Evaluation—Final Report," Report No. SAND86-8212, Sandia National Laboratories, Albuquerque, NM.

[2] Pacheco, J. E., Showalter, S. K., and Kolb, W. J., 2002, "Development of a Molten-Salt Thermocline Thermal Storage System for Parabolic Trough Plants," ASME J. Sol. Energy Eng., **124**, pp. 153–159.

[3] Yang, Z., and Garimella, S. V., 2010, "Thermal Analysis of Solar Thermal Energy Storage in a Molten-Salt Thermocline," Sol. Energy, **84**, pp. 974–985.

[4] Flueckiger, S. M., Yang, Z., and Garimella, S. V., 2012, "Thermomechanical Simulation of the Solar One Thermocline Storage Tank," ASME J. Sol. Energy Eng., **134**, p. 041014.

[5] Van Lew, J. T., Li, P., Chan, C. L., Karaki, W., and Stephens, J., 2011, "Analysis of Heat Storage and Delivery of a Thermocline Tank Having Solid Filler Material," ASME J. Sol. Energy Eng., **133**, p. 021003.

[6] Kolb, G. J., 2011, "Evaluation of Annual Performance of 2-Tank and Thermocline Thermal Storage Systems for Trough Plants," ASME J. Sol. Energy Eng., **133**, p. 031023.

[7] Flueckiger, S. M., Iverson, B. D., Garimella, S. V., and Pacheco, J. E., 2014, "System-Level Simulation of a Solar Power Tower Plant With Thermocline Thermal Energy Storage," Appl. Energ., **113**, pp. 86–96.

[8] Flueckiger, S. M., Iverson, B. D., and Garimella, S. V., 2013, "Simulation of a Concentrating Solar Power Plant With Molten-Salt Thermocline Storage for Optimized Annual Performance," Proceedings of the ASME 2013 7th International Conference on Energy Sustainability, Minneapolis, MN, July 14-19.

[9] Nissen, D. A., 1982, "Thermophysical Properties of the Equimolar Mixture $NaNO_3$-KNO_3 From 300 to 600 °C," J. Chem. Eng. Data, **27**, pp. 269–273.

[10] Cote, J., and Konrad, J.-M., 2005, "Thermal Conductivity of Base-Coarse Materials," Can. Geotech. J., **42**, pp. 61–78.

[11] Flueckiger, S. M., and Garimella, S. V., 2012, "Second-Law Analysis of Molten-Salt Thermal Energy Storage in Thermoclines," Sol. Energy, **86**, pp. 1621–1631.

[12] Wakao, N., and Kaguei, S., 1982, *Heat and Mass Transfer in Packed Beds*, Gordon Beach, New York.

[13] Gonzo, E. E., 2002, "Estimating Correlations for the Effective Thermal Conductivity of Granular Materials," Chem. Eng. J., **90**, pp. 299–302.

[14] Stoddard, M. C., Faas, S. E., Chiang, C. J., and Dirks, J. A., 1987, "Solergy," Report No. SAND86-8060, Sandia National Laboratories, Albuquerque, NM.

[15] Kistler, B. L., 1986, "A User's Manual for DELSOL3," Report No. SAND86-8018, Sandia National Laboratories, Albuquerque, NM.

[16] Pacheco, J. E., 2002, "Final Test and Evaluation Results From the Solar Two Project," Report No. SAND2002-0120, Sandia National Laboratories, Albuquerque, NM.

[17] Kolb, G. J., 2011, "An Evaluation of Possible Next-Generation High-Temperature Molten-Salt Power Towers," Report No. SAND2011-9320, Sandia National Laboratories, Albuquerque, NM.

[18] National Renewable Energy Laboratory, 2013, "Simple Levelized Cost of Energy (LCOE) Calculator," http://www.nrel.gov/analysis/

[19] Kolb, G. J., Ho, C. K., Mancini, T. R., and Gary, J. A., 2011, "Power Tower Technology Roadmap and Cost Reduction Plan," Report No. SAND2011-2419, Sandia National Laboratories, Albuquerque, NM.

[20] National Renewable Energy Laboratory, 2012, "System Advisor Model, Ver. 2012.11.30," https://sam.nrel.gov/

[21] Electric Power Research Institute, 2010, "Solar Thermal Storage Systems: Preliminary Design Study," 1019581, EPRI, Palo Alto, CA.

[22] U.S. Department of Energy, 2011, "SunShot Concentrating Solar Power (CSP) R&D," Report No. DE-FOA-0000595, DOE.